

RSC Advances



This is an *Accepted Manuscript*, which has been through the Royal Society of Chemistry peer review process and has been accepted for publication.

Accepted Manuscripts are published online shortly after acceptance, before technical editing, formatting and proof reading. Using this free service, authors can make their results available to the community, in citable form, before we publish the edited article. This *Accepted Manuscript* will be replaced by the edited, formatted and paginated article as soon as this is available.

You can find more information about *Accepted Manuscripts* in the [Information for Authors](#).

Please note that technical editing may introduce minor changes to the text and/or graphics, which may alter content. The journal's standard [Terms & Conditions](#) and the [Ethical guidelines](#) still apply. In no event shall the Royal Society of Chemistry be held responsible for any errors or omissions in this *Accepted Manuscript* or any consequences arising from the use of any information it contains.



Improving Thermal and Mechanical Properties of Epoxy Composites by Using Functionalized Graphene

Received 00th January 20xx,
Accepted 00th January 20xx

DOI: 10.1039/x0xx00000x

www.rsc.org/

Lulu Pan¹, Jianfeng Ban³, Shaorong Lu^{*1}, Guoxin Chen², Jin Yang¹, Qiyun Luo¹, Linyan Wu¹, Jinhong Yu^{*1,2}

Perylene tetracarboxylic anhydride (PTCDA) was reacted with 6-aminocaproic acid to form the corresponding perylene bisimide (PBI). PBI was used as foundation an oligomerisation of glycidol in a ring-opening reaction of glycidol leading to a hyper branched, water soluble glycidol derivative of perylene (PBI-HPG). PBI-HPG was bound to the reduced graphene oxide via π - π stacking resulting in a compound termed PBI-HPG/RGO. The structure and morphology of PBI-HPG/RGO were investigated by infrared spectroscopy (FT-IR), wide angle X-ray diffractometry (WAXD), transmission electron microscopy (TEM), atomic force microscope (AFM) and X-ray photoelectron spectroscopy (XPS). PBI-HPG/RGO was blended into at different loadings in order to improve the thermal and mechanical properties of epoxy composites. The maximum T_g of the epoxy composites was about 20 °C and the decomposition temperature (T_d) was 26 °C higher than that of neat epoxy. The incorporation of PBI-HPG/RGO yields a material with an impact strength of 39.6 KJ/m² and a tensile strength at 0.7 wt%. It increased by 50.8% and 62.3%, respectively, compared to the neat epoxy.

Introduction

Epoxy resins have many attractive properties such as good stiffness, creep resistance, high strength and modulus and good thermal stability.¹ Thus, their use is widespread used in coatings, adhesives and reactive diluents.² But there are some drawbacks such as the poor resistance to crack propagation and low toughness, which limit the applications of epoxy. Numerous efforts have been undertaken on improving the toughness of cured epoxy resin through introducing rigid particles, reactive rubbers, graphene or hyperbranched polymers.³

Reduced graphene oxide (RGO) is comprised of a single layer of aromatic carbon atoms. RGO has attracted considerable attention in recent years due to its mechanical strength, thermal conductivity and electrical mobility properties.^{4,5} RGO has been applied in various fields, such as microelectronic devices, energy-storage materials and fillers for conductive materials.^{6,7} The main features of composites involving RGO are their strength, quasi-static fracture toughness and electrical and

thermal properties compared to the neat polymer.⁷ The bottleneck in the application of RGO is its tendency for irreversible aggregation induced by strong van der Waals force.⁸ To ensure making full use of the properties of RGO, chemical modifications of RGO become necessary to improve the dispersion and interfacial force between RGO and polymer matrix.⁹ For example, covalent or non-covalent modification of the RGO can prevent their aggregation. However, covalent functionalization can alter the electronic structure of RGO. Therefore, non-covalent modification, such as π - π stacking interactions are preferred.⁶ In order to explore the cooperative π - π assembly between RGO and a planar aromatic molecule, we choose the perylene bisimide (PBI) as the organic molecule. The use of PBI is justified due to its chemical structure and thermal stability.¹⁰

Perylene bisimides have attracted attention in theoretical and applied research.¹¹ PBI have been used in n-type semiconductor materials, light collection, organic light-emitting devices and supramolecular self-assembly due to PBI's good thermal stability, chemical inertness and high fluorescence quantum yield.¹² Some attention has been focused on the modification of structure of perylene bisimide in order to improve the chemical and physical properties, such as its poor water-solubility.¹³ The perylene bisimide has a planar, benzene ring structure, thus it tends to assemble via noncovalent interactions, such as hydrogen bonding, van der Waals and π - π stacking interactions.^{10,14} Consequently it could bind well to RGO. However, the solubility of PBI is a hurdle in this application. A solution is offered by Haag and coworkers, who bound hyperbranched polyglycerol (HPG) onto the imide functionality of

¹Key Laboratory of New Processing Technology for Nonferrous Metals and Materials, Ministry of Education, School of Material Science and Engineering, Guilin University of Technology, Guilin 541004, China.

²Key Laboratory of Marine Materials and Related Technologies, Zhejiang Key Laboratory of Marine Materials and Protective Technologies, Ningbo Institute of Materials Technology and Engineering, Chinese Academy of Sciences, Ningbo 315201, China.

³Key Laboratory of Optoelectronic Devices and Systems of Ministry of Education and Guangdong Province, College of Optoelectronic Engineering, Shenzhen University, Shenzhen 518060, Guangdong Province, China. Email address: tushaor@163.com (S. R. Lu); yujinhong@glut.edu.cn (J. H. Yu).

PBI to form fluorescent and water-solubility PBI dyes. Their approach opportunities to fabricate compounds based on RGO and perylene bisimide in aqueous media.¹⁵ This pathway is especially promising as hyper-branched polyglycerol can be used to improve the toughness of cured epoxy resin in its own right due to the number of terminal groups/potential binding sites in HPG. The hydroxylic terminal groups can interact with epoxy, without sacrificing the intrinsic properties of HPG.¹⁶

Hyperbranched polyglycerols (HPGs) belong to a group of macromolecules known as dendrimers or dendritic polymers. The distinctive characteristics of HPG dendrimers is their highly branched structure containing many hydroxyl groups on the surface, which not only increases their solubility but also decreases their intrinsic viscosity.^{16,17} They have attracted considerable attention over the past few years due to their unique molecular structure and properties.¹⁸ HPGs can be synthesized via the anionic ring-opening reaction of glycidol. The advantages of this synthesis method are a simple “one-step” reaction, good control of the course of reaction, a narrow polydispersity and the ease at which HPGs can be modified with functional groups.^{19,20} In addition, HPGs have excellent water solubility and biocompatibility.¹⁸

we aimed to combine HPGs and perylene bisimides to prepare a hybrid material that can be used to bind to RGO and address its tendency to agglomerate. Such material brings to the compound the water-solubility of perylene bisimides and combined chemical and physical properties of both HPGs and PBI.²¹ The PBI-HPG was reacted with RGO in a self-assembly, functional groups on the RGO nanosheets via π - π stacking interactions. The resulting product was named PBI-HPG/RGO. PBI-HPG/RGO was incorporated into the epoxy resin and the mechanical and thermal properties of the composite were studied and compared to neat.

Experimental

Materials

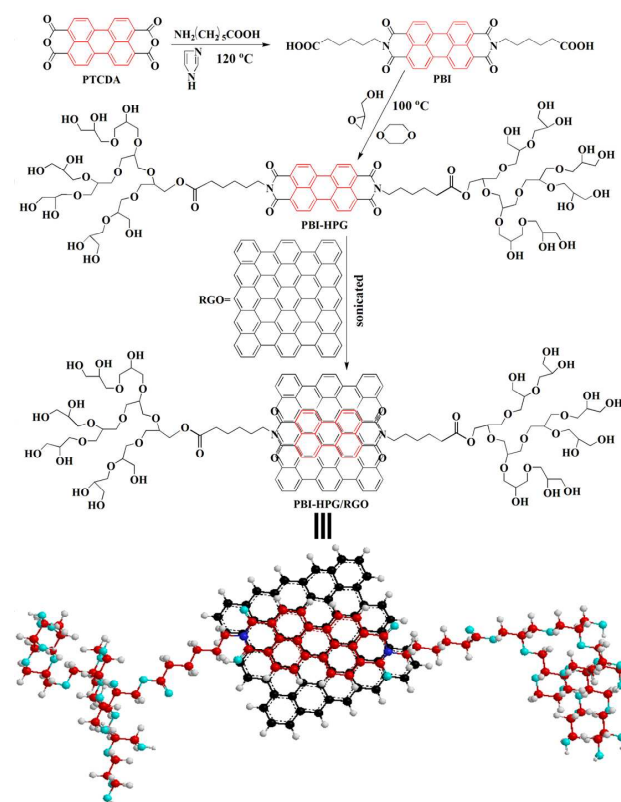
3, 4, 9, 10-Perylene tetracarboxylic anhydride (PTCDA) was obtained from Xiya Chemical Reagent Company (Chengdu, China). Nature flake graphite (325 mesh, 99%) was provided by Hengrui Graphite Co., Ltd. (Qingdao, China). H_2SO_4 (98%), HCl (36%), H_2O_2 (30%), KMnO_4 , P_2O_5 and $\text{K}_2\text{S}_2\text{O}_8$ were purchased from Sinopharm Chemical Reagent Co., Ltd. (Shanghai, China). Epoxy resin (diglycidyl ether of bisphenol A, with an epoxide equivalent weight of 227 g mol^{-1} and its epoxide value was 0.44, named E-44) was purchased from Yueyang Chemical Plant in China. 4, 4'-Diaminodiphenylsulphone (DDS) and dioxane were obtained from Sinopharm Chemical Reagent Co., Ltd., China. 6-aminocaproic acid, glycidol, imidazole and sodium hydride are all purchased from Aladdin. The solvent DMF and acetone were analytical grade, provided by Guanddong Guanghua Sci-Tech Co., Ltd, China. All other reagents and solvents were used as received without further purification.

Synthesis of the perylene bisimide derivatives (PBI)

3, 4, 9, 10-peryene tetracarboxylic anhydride (PTCDA) (1.5 g, 3.8 mmol), 6-aminocaproic acid (1.49 g, 11.4 mmol) and imidazole (16 g) were placed into a 250 mL round bottomed three-neck flask equipped with nitrogen inlet and thermometer. The mixture was purged with nitrogen for 15 min before being kept at 120°C for 12h. Then the reaction mixture was cooled to 90°C and deionized water was added under nitrogen.²² After stirring at 90°C for 2 h, the dark-red solution was filtered to remove the unreacted PTCDA. The solution was acidified with 2 M HCl aqueous solution until the PH value was between 3 and 4. Then the dark-red precipitate was washed with deionized water until the filtrate was at a nearly neutral pH value.²³ The product was dried at 60°C in a vacuum drying oven to gain a red brown powder.

Preparation of HPG perylene bisimide derivatives (PBI-HPG)

The reaction was carried out in a three-neck flask equipped with nitrogen inlet and thermometer. The compound PBI (0.1 g) was added to a suspension of sodium hydride (0.015 g) in DMF, and then stirred for 1 h at 70°C . A total of 2 mL of anhydrous dioxane was added. Then mixture was heated to 100°C and glycidol was added dropwise over a period of 12 h to the deprotonated compound PBI at 110°C for another 12 h.²⁴ After reaction, the mixture was cooled to the room temperature and quenched by methanol. Subsequently the product was centrifuged and washed several times with methanol. The product marked as PBI-HPG was dried at 60°C in a vacuum oven to constant weight.



Scheme 1 The preparation process of the PBI-HPG/RGO.

Preparation of PBI-HPG/RGO

Firstly, the graphene oxide (GO) was prepared according to the modified Hummers method, then the reduced graphene oxide (RGO) was obtained by thermal annealing of GO to 1100 °C at a heating rate of 2 °C min⁻¹ under a 3% H₂/Ar stream for 12 h. Secondly, the as-made RGO nanosheets were dispersed in DMF and sonicated for 30 min.²⁵ Then PBI was added and the mixture sonicated for another 30 min. The mass ratio of PBI-HPG to RGO was 3:1. After that, the mixture was refluxed in a three-necked flask under nitrogen protection at 100 °C for 24 h. After completion of the reaction, the product was washed with DMF/ethanol several times and centrifuged at 9500 rpm to remove unreacted PBI-HPG. The dark solid product marked as PBI-HPG/RGO was dried overnight under vacuum at 60 °C. The synthetic route is shown in **Scheme 1**.

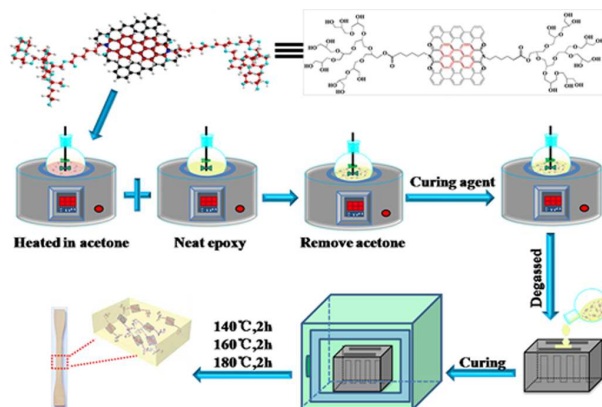
Preparation of epoxy composites

The epoxy composites were prepared as follows. Firstly, 26 g epoxy was placed into a round bottom flask and stirred and degassed at 70 °C. Secondly, a certain quantity (see below) of PBI-HPG/RGO was ultrasonic dispersion in acetone for 20 min at room temperature. Then the PBI-HPG/RGO acetone suspension was added to the pretreated epoxy slowly under stirring. The temperature of the reaction mixture was raised to 70 °C and mixture was stirred for 30 min to ensure good homogeneity and remove the acetone entirely. Thirdly, 7.8 g DDS as curing agent was added under vigorous mechanical stirring. The mixture was degassed until no more bubble formation was observed. Finally, the mixture was poured into preheated stainless steel molds and degassed in an oven at 130 °C for 30 min. The mold was placed in a convection oven to cure at 140 °C for 2 h, 160 °C for 2 h and 180 °C for 2 h. PBI-HPG/RGO was added at different weight fractions (0.1, 0.5, 0.7 and 1.0 wt%) by above methods. The details of the preparation of the epoxy composites are shown in **Scheme 2**.

Characterization

Fourier transform infrared spectra (FT-IR) were recorded on a Thermo Nexus 470 FTIR spectrometer (KBr disk). Powder X-ray diffraction (XRD) patterns were recorded using a Holland PANalytical X-Pert PRO X-ray diffractometer. Thermogravimetric analysis (TGA) instrument (Netzsch STA-449) was used to probe the thermal stability up to 800 °C at a scanning rate of 10 °C min⁻¹. ¹HNMR measurements were conducted on a Bruker ARX400 MHz spectrometer using tetramethylsilane (TMS) as the internal standard at ambient temperature. The T_g measurements of epoxy composites were performed on a Netzsch DSC-204 differential scanning calorimetry spectrometer with a heating rate of 20 °C min⁻¹ in nitrogen atmosphere. XPS measurement was recorded with a ESCALAB 250Xi instrument (Thermo Electron Corporation, US). UV-Vis spectra in the wavelength range of 300-700 nm was obtained from a UV 3600 spectrophotometer (SHIMADZU Company, Japan). The zeta potential of final product was estimated from a Nanoparticle & Zeta Potential Analyzer (ZS90). AFM images were taken on a Ntegra Prima SPM Scanning Probe Microscope (NT-MDT, Russia). Field emission scanning electron microscope (FE-SEM, JEOL JEM-6610) was used to observe the morphology of the specimens. Transmission electron microscopy (TEM) images

were recorded on a JEM-2100F high-resolution transmission electron microscope at 200 kV. Samples were prepared by placing a drop of dilute ethanol dispersion on the surface of a micro-grid. The morphologies and the corresponding height profiles of the samples were studied via SPM-9600 atomic force microscopy (Shimadzu, Japan). Thermal infrared images on neat epoxy and its composites were taken by thermo tracer TH6200 (NEC, JAPAN). The storage modulus was performed on a DMA Q800 dynamic mechanical analyzer (TA Instruments, USA). Mechanical properties of the composites were evaluated by impact, tensile and flexural measurements. The impact strength of the cured samples was measured on a tester of type XJJ-5 according to National Standard of China (GB1043-79). The size of cured specimen was trimmed into a dimension of 80 × 10 × 4 mm for testing. The tensile strength was examined on a universal tensile tester of type RGT-5 according to National Standard of China (GB1040-92) at a rate of 2 mm min⁻¹. Flexural tests were performed by WDW-20 according to a three-point bending mode of the universal testing machine at a crosshead speed of 2 mm min⁻¹. The test results are the average value of five specimens and the testing temperature was room temperature.



Scheme 2 The preparation process of epoxy composites.

Results and discussion

Characterization of PBI-HPG/RGO

The FT-IR spectra of PBI, PBI-HPG, RGO and PBI-HPG/RGO are shown in **Fig.1(a)**. The FT-IR spectrum of PBI exhibited a characteristic absorption band at 1693 cm⁻¹, which was assigned to imide C=O stretching. Upon reaction of perylene tetracarboxylic anhydride with 6-aminocaproic acid to form PBI absorbance bands of hydroxyl functional group (3428 cm⁻¹) and aliphatic C-H group (2926 cm⁻¹ and 2856 cm⁻¹) can be observed. The band at 3428 cm⁻¹ can be explained by the overlap between free hydrogen bond and N-H stretching vibration. Thus these characteristic absorption bands indicated the reaction between perylene and 6-aminocaproic acid. Several new peaks were observed in the FT-IR spectrum of the PBI-HPG. The band at 1726 cm⁻¹ corresponded to an ester bond which was formed by the reaction of hydroxyl group of glycidol and carboxylic groups at the end of PBI.²⁶ The typical

absorbance peaks appearing at 1120 cm^{-1} – 1075 cm^{-1} could be attributed to C-O bonds. It confirmed that glycidol had successfully reacted with PBI via ring opening reaction.²⁷ In the spectra of the RGO the absorbance band of aromatic C=C bonds of graphene was in the 1570 cm^{-1} – 1690 cm^{-1} region. The presence of RGO was confirmed by FT-IR where there was no oxygen functionality except -OH group which might be due to incomplete reduction of GO as shown in spectra at 3431 cm^{-1} .²⁸ Comparing the spectra of PBI-HPG and PBI-HPG/RGO it can

be seen that the intensity of the peaks at 1729 cm^{-1} and 1120 cm^{-1} – 1075 cm^{-1} region gradually became weak due to the π - π stacking interactions between the RGO and PBI-HPG.²⁷ The bulk of the RGO impeded some further groups, which decreased the intensity of the signals associated with their bonds. Other absorbance peaks didn't change or shift too much compared to the spectrum for PBI-HPG. This indicated that PBI-HPG/RGO was successfully synthesized.

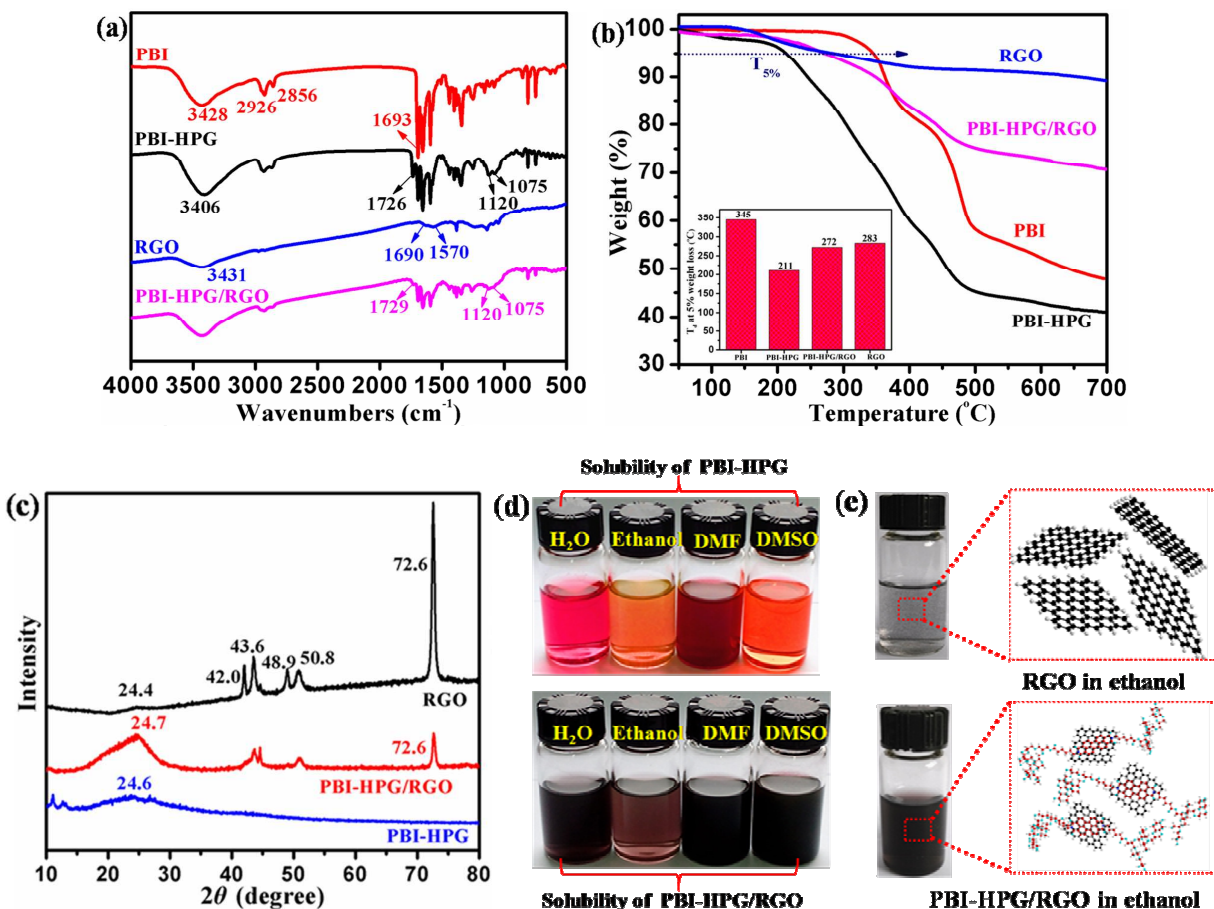


Fig. 1 (a) FT-IR spectra and (b) TGA curves of PBI, PBI-HPG, RGO and PBI-HPG/RGO. (c) WAXD curves of RGO, PBI-HPG and PBI-HPG/RGO. (d) Solubility of PBI-HPG and PBI-HPG/RGO in H_2O , ethanol, DMF and DMSO, respectively. (e) The dispersion of RGO, PBI-HPG/RGO in ethanol.

Thermal stability is an important property for potential applications. The TGA curves of the each product is scrutinized and shown in **Fig. 1(b)**. It can be seen from **Fig. 1(b)**, the initial decomposition temperature of the PBI was about $300\text{ }^{\circ}\text{C}$, which was attributed to the loss of alkyl chain segment belonging to 6-aminocaproic acid in the molecule. It indicated that the addition of alkyl chain segment could reduce the decomposition temperature. The final decomposition temperature was at around $500\text{ }^{\circ}\text{C}$, which was the decomposition of benzene ring of the perylene bisimide. RGO kept stable over a wide temperature range, and exhibited good thermal stability. RGO lost only 8.3% weight due to the pyrolysis of the residual oxygen-containing functional groups at $400\text{ }^{\circ}\text{C}$. From the curve

of PBI-HPG can be seen, the major weight loss occurred between $200\text{ }^{\circ}\text{C}$ and $480\text{ }^{\circ}\text{C}$. It could be attributed to the loss of glycidol units from the HPG units of PBI-HPG.²⁹ The main degradation stage ended at about $500\text{ }^{\circ}\text{C}$ and the residue yield calculated at $700\text{ }^{\circ}\text{C}$ was about 40 wt%. As shown in the TGA curve of PBI-HPG/RGO, addition of RGO had a stabilising effect on PBI-HPG. PBI-HPG/RGO decomposed at higher temperatures than PBI-HPG. As can be seen in **Fig. 1(b)** the main weight loss occurred between $230\text{ }^{\circ}\text{C}$ and $480\text{ }^{\circ}\text{C}$ and the residue yield calculated at $700\text{ }^{\circ}\text{C}$ was about 70 wt% of its total weight. These changes suggested that the product PBI-HPG/RGO was successfully synthesized.

The wide-angle X-ray diffraction (WAXD) patterns of RGO, PBI-HPG and PBI-HPG/RGO are shown in **Fig.1(c)**. The WAXD results indicated interlayer spacing and stacking between the PBI-HPG and RGO. The RGO pattern showed four reflections at $2\theta = 24.4^\circ$, $2\theta = 42.0^\circ\sim 43.6^\circ$, $2\theta = 48.9^\circ\sim 50.8^\circ$ and $2\theta = 72.6^\circ$. The pattern confirmed that the RGO had crystalline structure and ordered arrangement. The weak broad reflection at around 24° was characteristic for RGO.^{30,31} The value at about $2\theta = 43^\circ$ could be assigned to the [100] plane of graphene nanosheets.³² The PBI-HPG pattern showed a broad reflection at about $2\theta = 24.6^\circ$ which suggested that PBI-HPG was disordered and X-ray amorphous or polycrystalline. It conformed to the structural properties of hyperbranched polymer.⁴

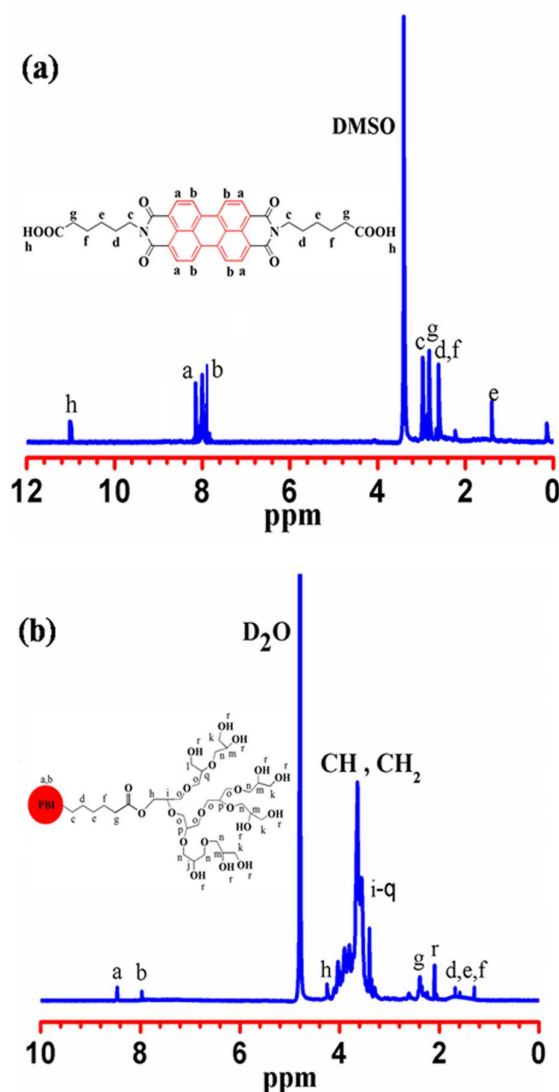


Fig.2 $^1\text{H-NMR}$ spectra of (a) PBI and (b) PBI-HPG.

The pattern of PBI-HPG/RGO was a combination of patterns of RGO and PBI-HPG. The intensity of some reflections was distinctly weakened compared to RGO, which illustrated that

the amorphous PBI-HPG had stacked onto the RGO nanosheets and the hyperbranched polymer might weaken the diffraction intensity through the dilution effect of polymer chains.^{28,33} So the PBI-HPG was less crystalline than RGO. The wide-angle X-ray diffraction experiment proved the successful stack between PBI-HPG and RGO. The optical photographs of PBI-HPG and PBI-HPG/RGO solution are shown in the **Fig.1(d)**. The PBI-HPG dissolved well in distilled water and DMSO. **Fig.1(e)** shows the RGO and PBI-HPG/RGO dispersion in ethanol. From the images could be concluded that the dispersion of RGO could be improved by the joining of PBI-HPG via π - π stacking force.

$^1\text{H-NMR}$ spectrum provided more detailed evidence to prove that PBI and PBI-HPG successful synthesis, as depicted in **Fig.2**. As can be seen in **Fig.2(a)**, the characteristic peaks in the chemical shift region 7.89-8.23 ppm from the aromatic protons was clearly detected in the $^1\text{H-NMR}$ spectra of PBI. The signal at 11 ppm, associated with the carboxylic acid proton is weak as expected for an exchangeable proton. The $^1\text{H-NMR}$ results were compared with the literature data, thereby it further confirmed the correct structure.^{23,34} The characterization data of PBI were as follows: $^1\text{H-NMR}$ (ppm, DMSO): 10.99 (s, 2H, COOH), 7.89-8.23 (s, 8H, ArH), 2.43-2.94 (s, 16H, $-\text{CH}_2-$), 1.28 (s, 4H, $-\text{CH}_2-$). The $^1\text{H-NMR}$ spectrum of PBI-HPG, as shown in **Fig.2(b)**, shows that the proton resonances belonging to $-\text{OH}$ of the PBI-HPG could be found at 2.09 ppm and the proton resonances of $-\text{CH}_2-$ and $-\text{CH}-$ of hyperbranched polyglycidyl were observed at 3.49-4.23 ppm.²⁴ In addition, the aromatic protons peaks of the PBI-HPG at 8.46 ppm and 7.95 ppm were very weak. And the protons of $-\text{CH}_2-$ belonging to 6-amino caproic acid were at 1.30-2.38 ppm. The $^1\text{H-NMR}$ results confirmed the correct structure. The characterization data of PBI-HPG were as follows: $^1\text{H-NMR}$ (δ , ppm, D_2O): 8.46-7.95 (s, 8H, ArH), 3.49-4.23 (s, 88H, $-\text{OCH}_2-$ and $-\text{CH}-$), 2.09 (s, 20H, $-\text{OH}$), 1.30-2.38 (s, 20H, $-\text{CH}_2-$).

Fig.3(a) shows the zeta potential of the PBI-HPG/RGO measured at different pH in distilled water. The zeta potential of PBI-HPG/RGO was recorded in the range from about -3 mV (acidic conditions) to about -40 mV (alkaline conditions). The curve indicated that the surface of PBI-HPG/RGO was negatively charged when dispersed in distilled water even at low pH values. With the increase in alkali the quantity of negative charge increased. This was attributed to the high ionization of the hydroxyl groups originated from the PBI-HPG.³⁵ It suggested that the formation of stable PBI-HPG/RGO colloids in aqueous solution was due to the electrostatic repulsion.

Fig.3(b) shows a comparison of UV-vis absorption spectra of PBI-HPG, PBI-HPG/RGO and RGO dispersed in aqueous solution. The spectrum of the PBI-HPG in distilled water showed three characteristic absorption peaks at 470, 499 and 547 nm, which corresponded to the electronic transitions of PBI-HPG.³⁶ However, the three characteristic absorption peaks in the spectrum of PBI-HPG/RGO had a slight shift, and these peaks did not appear in the spectrum of the RGO. The peaks were red shifted by about 10 nm comparing to the spectrum of PBI-HPG. This was consistent with the presence of π - π

stacking interactions between the PBI-HPG moieties and the RGO nanosheets.² Thus it further evidenced that the RGO had successfully stacked with PBI-HPG via π - π intermolecular forces.

The X-ray photoelectron spectroscopy (XPS) spectra of the PBI-HPG/RGO showed peaks corresponding to the binding energies of about 284 eV, 399 eV and 531 eV which were attributed to C 1s, N 1s and O 1s energy levels, respectively (Fig.3c-d). A strong O 1s signal appeared in Fig.3(c), suggesting that the PBI-HPG/RGO contained oxygen, which is most likely located in the glycidol groups. The XPS spectrum

shows no other elements to be present, indicating the by-products had been washed out during processing.³⁷ The C 1s core-level spectrum of PBI-HPG/RGO (Fig.3(d)) could be fitted into five components with BEs at about 283.6, 285.0, 285.8, 287.0 and 288.3 eV. These could be attributed to the sp^2 hybridized carbon, C-C/C-H, C-O-C/C-OH, N-C=O and O-C=O species, respectively.^{37,38} And the C-O-C/C-OH originated from the hyperbranched polyglycerols moieties of PBI-HPG. The N 1s signal (shown in inset of Fig.3(d)) was consistent with the PBI-HPG/RGO. The XPS data confirmed that PBI-HPG covered the surface of RGO nanosheets.

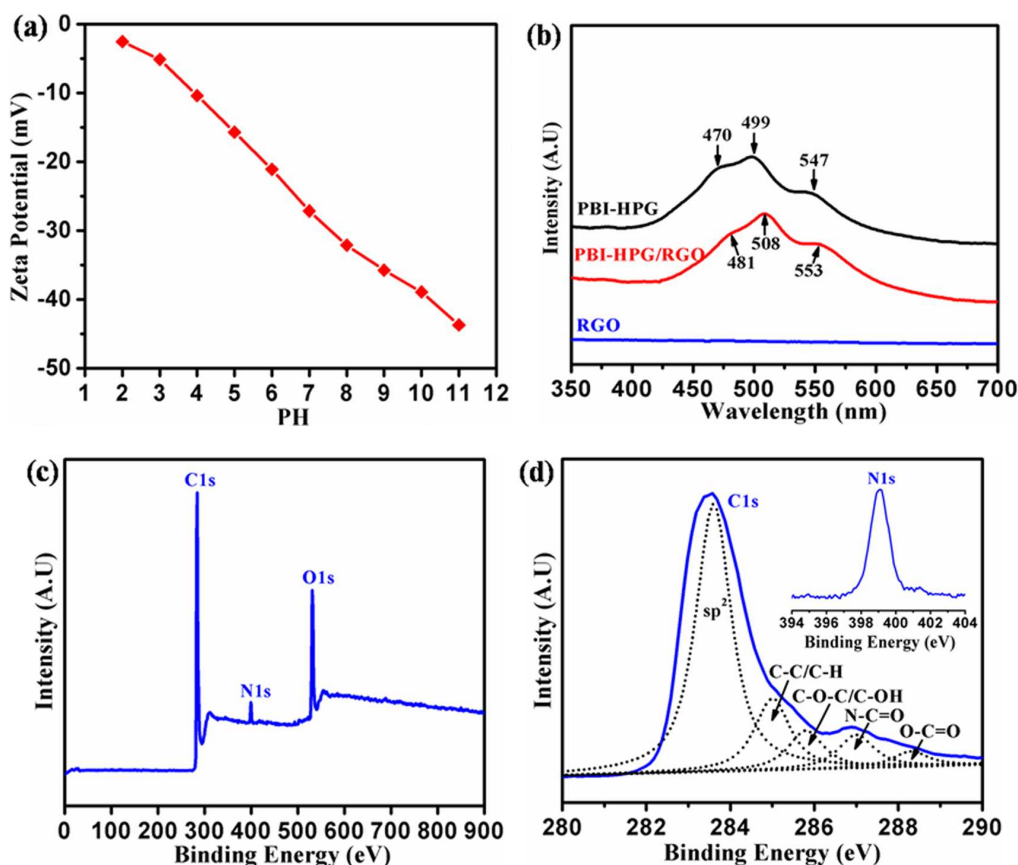


Fig.3 (a) Zeta potential of PBI-HPG/RGO dispersion in distilled water. (b) UV-Vis spectra of PBI-HPG, RGO and PBI-HPG/RGO. (c-d) XPS wide scan and C 1s core-level spectra of the PBI-HPG/RGO.

Fig.4(a) shows typical AFM images and the height profiles of RGO and PBI-HPG/RGO dispersed in ethanol, cast onto cleaved mica dried under vacuum at room temperature. The average thickness of RGO was determined to be about 3.5 nm from the height profile of AFM image suggesting a single layer structure.³⁹ However, the thickness was still larger than the theoretical value of a perfectly carbon-carbon bond (sp^2) thickness in graphene.⁴⁰ The result was attributed to the inherent deformation of graphene as well as the instrumental offset of the AFM probe within the range of allowable error.⁴¹ The thickness of PBI-HPG/RGO was tested by AFM and the image is shown in **Fig.4(b)**. In the microscope image a cross-section of a flake could be observed showing RGO with

thickness of about 8.5 nm, which indicated the RGO had two or three layers stacked together. In the literature this was assumed to be due to the interactions between PBI-HPG unites.²⁷ Because the perylene bisimide has a benzene ring structure, so it could bind to RGO via π - π stacking. Thus the thickness of PBI-HPG/RGO is not only due to stacking but also due to the PBI-HPG added. From the height profiles of PBI-HPG/RGO could be seen, the height increases was much larger than expected for a single or stacked sheet of RGO. The thickness difference between stacked and un-stacked area was about 16 nm on average,⁴² which was the thickness of PBI-HPG. The irregularity of hyperbranched polymer resulted in rough topology of PBI-HPG/RGO.⁴³ Hence, we could confirm that the

PBI-HPG/RGO had been successfully π - π stacked on the surface of RGO, while the edges of RGO nanosheets were free.

Fig.4(b) shows the transmission electron microscopy (TEM) image of RGO and PBI-HPG/RGO. The samples were dissolved in ethanol and distilled water respectively. Then one drop of the ethanol suspension was placed on the micro-grid. From the RGO picture can be seen, the edge of RGO sheet appeared to be rolled up and crumpled, which was attributed to its intrinsic nature.^{28,44} The morphology of PBI-HPG/RGO looked folded, indicating the π - π stacking interactions between RGO and PBI-HPG didn't alter the morphology of nanosheet RGO.² Some irregular dark shadow were noted (indicated by arrows) on the surface of nanosheet RGO. These could be interpreted as traces of PBI-HPG stacked on RGO via strong π - π interaction.^{24,38}

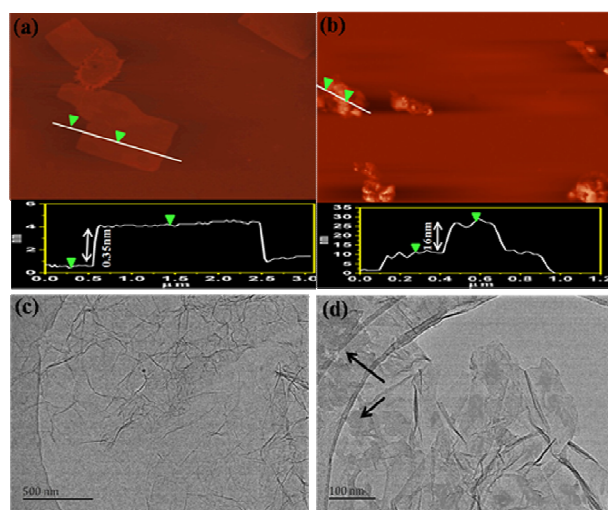


Fig.4 AFM images and TEM images of (a,c) RGO and (b,d) PBI-HPG/RGO.

Morphology of composites

The SEM images of fracture surfaces of the epoxy composites with different enlargement fractions after tensile tests are shown in **Fig.5**. It can be observed clearly from **Fig.5(a)** that several river-like lines appeared on the fracture surface of the neat epoxy. Single crack propagation is highlighted by an arrow in **Fig.5(a-b)**, which indicated that the structural deformation was brittle fracture. However, the fracture surfaces of modified epoxy composites were rougher with many cracks in **Fig.5(c-j)**. The mode of crack propagation was similar (seen in **Fig.5(c-j)**). The presence of RGO should produce some micro-cracks. It lead to the fracture surface roughness and irregularity. In particular, the crack became more clearly and deeper when the filler content was 0.7 wt%. This was attributed to the covalent reaction between the epoxy matrix and the hydroxyl groups of the PBI-HPG/RGO,⁴⁵ which provided strong interfacial interaction between PBI-HPG/RGO and the epoxy matrix.³⁶ Moreover, the degree of tough fracture reduced as the loading content increased, which can be seen in **Fig.5(i-j)**. The SEM analysis was confirmed by TEM micrograph of the epoxy

composites with 1.0 wt%, as shown in **Fig. S1**. Aggregation and poor dispersion explained the reduction in mechanical properties.

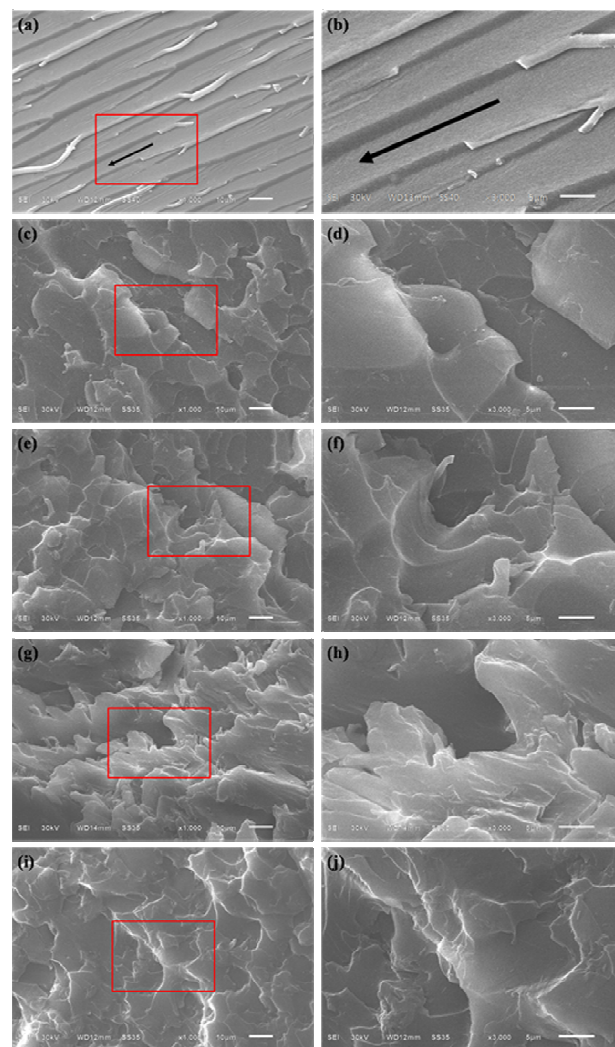


Fig.5 SEM images of fractured surface of composites with different enlargement fraction: (a- b) neat epoxy, (c - d) 0.1 wt%, (e - f) 0.5 wt%, (g - h) 0.7 wt%, (i - j) 1.0 wt%.

Thermal properties of composites

Fig.6 shows the behaviors of the thermal degradation of epoxy composites and the analyzed data are listed in **Table 1**. As shown in **Fig.6(a)**, the curves displayed one-step degradation mechanism indicating that addition of PBI-HPG/RGO did not change the degradation mechanism of the epoxy composites. The initial decomposition temperature (T_d) improved with the content of PBI-HPG/RGO increasing. The temperature at which a sharp weight loss occurs is an important parameter to prove the thermal stability of composites, which is denoted as decomposition temperature (T_d). The T_d of neat epoxy was lower than epoxy composites. And the temperature at weight loss of 5% (T_5) increased from 350 °C to 375 °C. **Fig.6(b)** shows the maximal decomposition temperature of epoxy

composites. The maximal decomposition temperature increased from 395 °C to 410 °C. It might be that PBI-HPG/RGO and epoxy resin participated in the formation of the crosslinked network.⁴⁶ Thus addition of RGO was effective in improving the thermal performance of epoxy composites. In addition, it was found that the dispersion between PBI-HPG/RGO and epoxy matrix and gas inclusions were important factors in determining the thermal properties of the composites. Volatile gas is less likely to be encapsulated and form pockets in the well dispersed mixtures.⁴⁷ The thermal stability increased initially but decreased if the additive content was more than 0.7 wt%, reaching a critical saturated state at this percentage. This was attributed to the huge volume of the hyperbranched polymer PBI-HPG/RGO, which generated a steric hindrance effect.⁴⁸ So hydroxyl groups in PBI-HPG/RGO were difficult to react with surface groups of epoxy resin or curing agent.

The glass transition temperatures of epoxy composites filled with PBI-HPG/RGO could be derived from DSC heating scans shown in Fig.7. The T_g of neat epoxy was lower than that of epoxy composites. The highest value 182.9 °C (0.7 wt% epoxy composite) and the lowest value 162.5 °C (neat epoxy) varied by about 20 °C. This was due to the fact that the hyperbranched polymer had lots of functional groups which could react with the groups of epoxy resin. From the curves, T_g increased up to the maximum value when filler content is 0.7 wt% and then decreased afterwards. RGO with its sheet morphology was an important factor for improving T_g at low filler loading. Because both the wrinkled structure and large specific surface area of RGO sheets likely induced strong interfacial interactions with polymer chains and larger influence on the thermal properties of the epoxy composites.⁴⁵ Further, good dispersion of RGO sheets lead to the formation of an interphase around each sheet in which the mobility of chains was constrained. Thus addition of PBI-HPG/RGO improved the T_g of the epoxy matrix. Otherwise, when filler content exceeded 0.7 wt%, the T_g decreased slightly. This might be due to localized clustering, which allowed the chain segments to move easily and thus decreased the T_g . Another reason was that the decreased degree of cross-linking induced by partial reaction of the curing agent led to a drop in T_g .⁴⁹ Thus these factors affected the glass transition temperature. The thermal properties of epoxy composites have been improved by PBI-HPG/RGO compound.

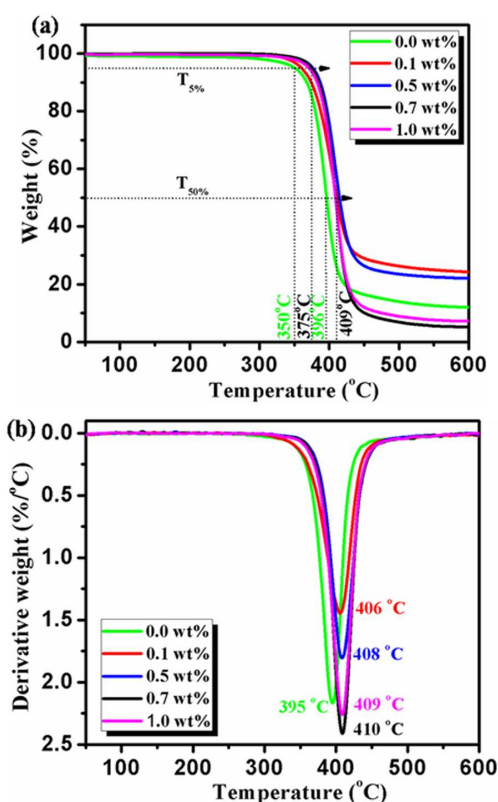


Fig.6 (a) TGA curves and (b) DTG curves of epoxy composites.

Table 1 Thermal stability of the composites calculated from TGA curves.

The content of PBI-HPG/RGO	Temperature at weight loss of 5% (T_5)	Temperature at weight loss of 50% (T_{50})	Char yield at 600 °C (%)
0.0 wt%	350	396	12%
0.1 wt%	360	411	24%
0.5 wt%	376	415	22%
0.7 wt%	375	409	5%
1.0 wt%	371	408	7%

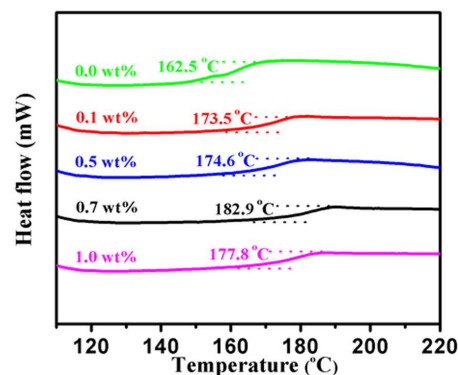


Fig.7 DSC curves of the epoxy composites.

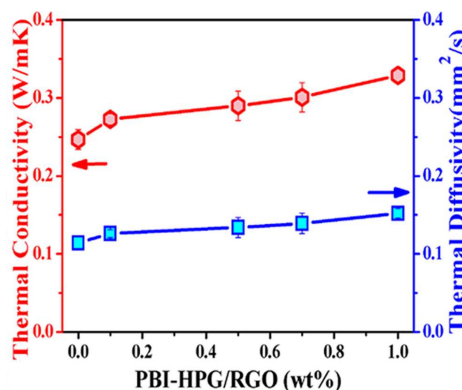


Fig.8 Thermal conductivity and thermal diffusivity of the epoxy composites.

The thermal conductivity and diffusivity of the fabricated epoxy composites containing PBI-HPG/RGO were examined as a function of the PBI-HPG/RGO content and the results are shown in Fig. 8. It was evident that the thermal conductivity increased steadily with the incorporation of the PBI-HPG/RGO. The thermal diffusivity of the epoxy composites showed a similar trend. This tendency of increase promised higher thermal conductivity higher loadings of PBI-HPG/RGO.

The thermal conductivity of neat epoxy was around 0.24 W/mK. The thermal conductivity of epoxy composites with the 1 wt% PBI-HPG/RGO was 0.33 W/mK, which is slightly higher than

that of the neat epoxy. It is known that the thermal conductivity is related to the loading, dispersion of fillers and the thermal resistance of interface between the fillers and matrix.⁵⁰ This phenomenon might be attributed to filler loading factors. The PBI-HPG/RGO filler were well dispersed in the epoxy composites, resulting in a strong interface thermal resistance between the fillers and epoxy matrix. Further comparison of the heat dissipation between the neat epoxy and its composites was performed using infrared imaging technology, as shown in Fig. S2 and Fig. S3.

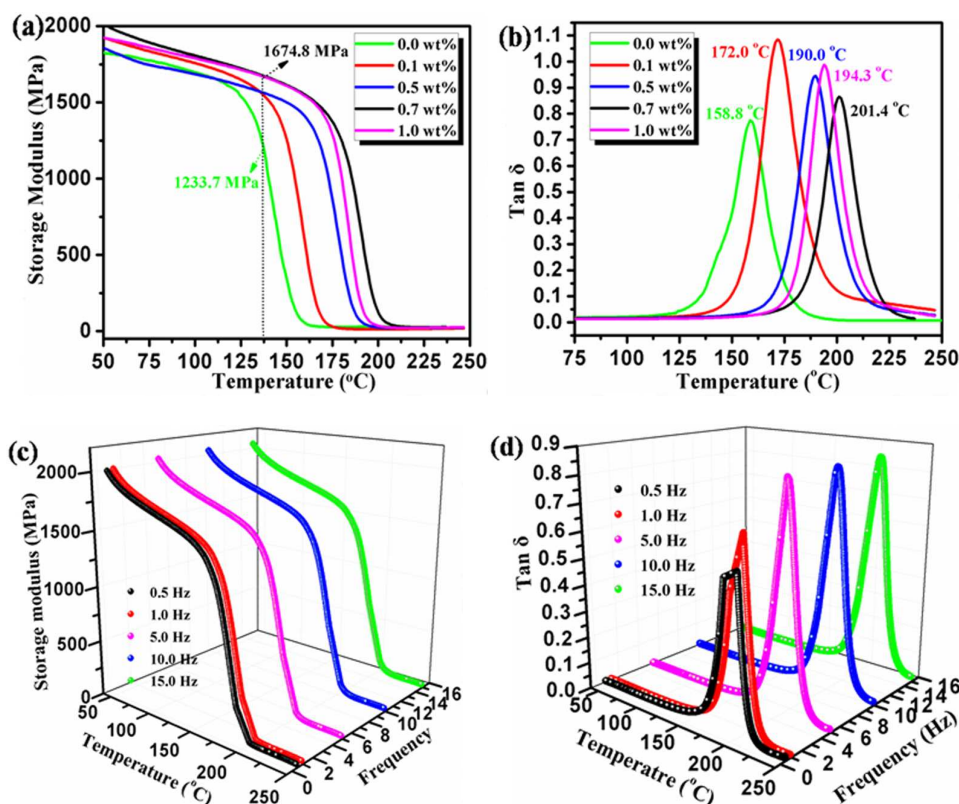


Fig. 9 (a) The storage modulus and (b) $\tan \delta$ of epoxy composites at 1 Hz frequency. (c-d) Different frequencies testing of epoxy composite with 0.7 wt% PBI-HPG/RGO.

Fig. 9 exhibits dynamic mechanical spectrum of different mass fraction epoxy composites, which shows the storage modulus and $\tan \delta$. The storage modulus and $\tan \delta$ rose with increasing amounts of filler. As can be seen in Fig. 9(a), it was found that storage modulus of neat epoxy was lower than that of the epoxy composites. The storage modulus of the epoxy composites decreased with an increase in temperature. This was attributed to the energy dissipation due to the mobility and movement of the polymer chains.⁵¹ However, the storage modulus increased with the addition of the filler's content over the whole temperature range. And the storage modulus curves of composites shifted to higher temperatures after addition of the PBI-HPG/RGO. The addition of 0.7 wt% PBI-HPG/RGO produced a significant increase of 35.8% from 1233.7 to 1674.8 MPa in the storage modulus at about 137 °C. It can be surmised

that the filler was conducive to improve the storage modulus of epoxy composites.

Fig. 9(b) shows $\tan \delta$ values of epoxy composites. In a sense, the $\tan \delta$ was equivalent to glass transition temperature (T_g). From the curves we can see, the T_g of the neat epoxy and its composite with 0.7 wt% PBI-HPG/RGO were 158.8 °C and 201.4 °C, respectively, which increased by about 42.6 °C. The storage modulus or T_g both followed the trend of reaching a maximum with the increasing filler content. This could be attributed to the following two factors: The cross-linking density was an important indicator for the impact strength and thermal performance. Because the cross-linking density dampened the motion of polymer chain and reduced free volume, it could increase the storage modulus and $\tan \delta$. However, once the cross-linking density exceeded a critical

value it resulted in phase separation and formation of reactive sites. Thereby it was impairing the cross-linking reaction between epoxy resin and compound PBI-HPG/RGO.⁵² The second factor is the dispersion of the filler in the resin. The dispersion was good at low filler contents, but declined when the content exceeded 0.7 wt% due to agglomeration of excess filler particles. **Fig.9(c-d)** displays the dynamic mechanical performance under different frequencies of epoxy composites with 0.7 wt% PBI-HPG/RGO. The energy storage modulus

increased with increasing frequency. But the amplitude of growth was not very consistent. Thus the conclusion was that the influence of frequency on the storage modulus was not as important as the dispersion and the cross-linking. Based on these findings, it was suggested that a low amount (0.7 wt%) of the compound PBI-HPG/RGO could improve the thermodynamic performance of epoxy resin.

Mechanical properties of composites

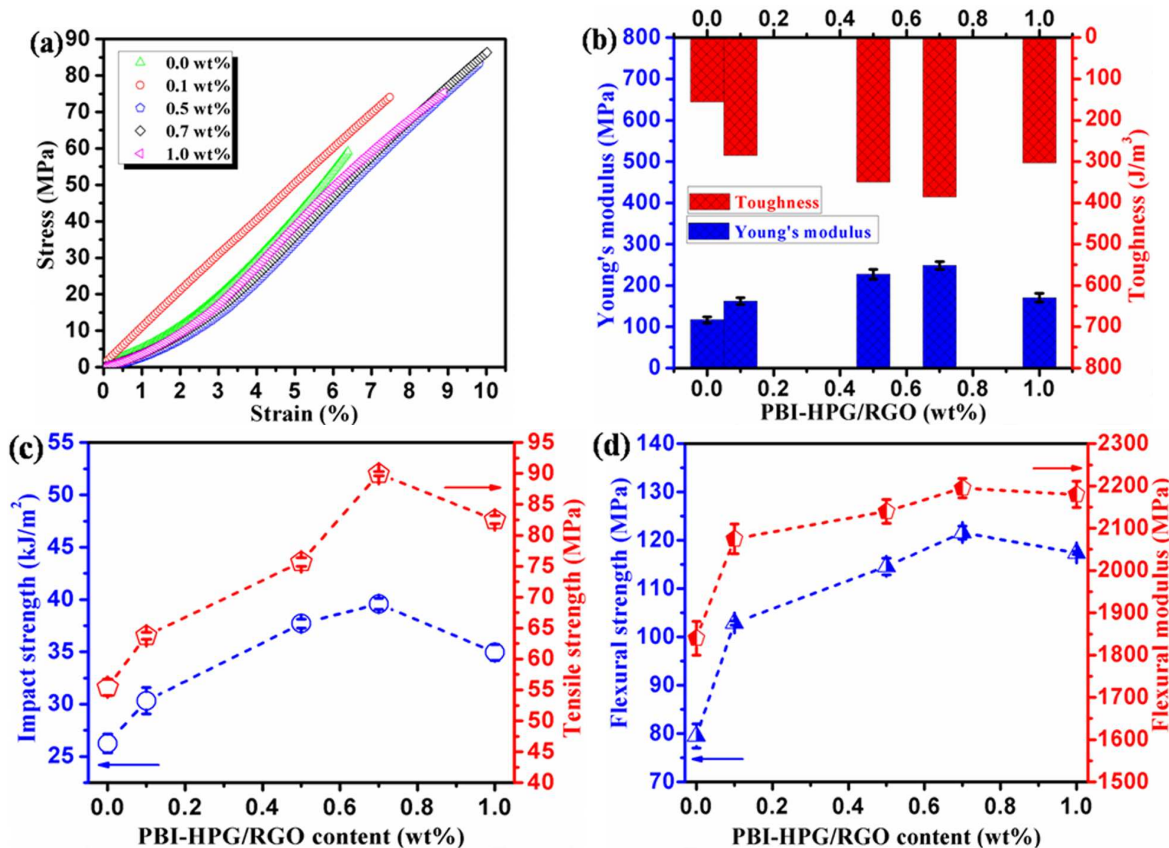


Fig.10 (a) Typical stress-strain curves, (b) Young's modulus and toughness, (c) Impact strength and tensile strength and (d) Flexural strength and modulus of the epoxy composites.

Fig.10(a) exhibits the stress strain behaviors of the epoxy composites. The epoxy composites showed the brittle deformation and present the tendency of linear growth upon the breaking point. It could see that the tensile properties of epoxy composites have been improved by the additive PBI-HPG/RGO. However, the tensile properties increased with the increment of filler until the weight percentage was 0.7 wt%. In comparison the tensile strength of the 1.0 wt% sample was marginally lower. Too much filler lead to the performance degradation of modified epoxies because the tensile loading caused stress concentration around filler particle until dissipation of the energy by sample deformation.⁵³ Another reason was that excessive filler content caused uneven dispersion, leading to phase separation. From **Fig.10(b)**, the toughness of neat epoxy was 155.2 J/m³ and increased up to 385.6 J/m³ upon addition of

PBI-HPG/RGO. It increased by 148.5% compared to the neat epoxy. The impact strength and tensile strength of different weight percentage of epoxy composites are shown in **Fig.10(c)**. The impact strength and tensile strength reached a maximum at a filler content of 0.7 wt% with values of 39.6 KJ/m² and 90.0 MPa, respectively, corresponding to improvements 50.8% and 62.3%, respectively. The reason for the improvements was thought to be the cross-linking reaction between epoxy groups and hydroxyl groups of hyperbranched polyglycidyl. The properties decayed slightly when the weight percentage of filler exceeded 0.7 wt%. This was attributed to bad dispersion inducing defects in the epoxy matrix.

The bending performance of the samples is shown in **Fig.10(d)**. From the graph in figure could be concluded that the flexural strength and modulus of epoxy composites were increased

compared to neat. The flexural strength of neat epoxy was 79.5 MPa and up to 121.6 Mpa for the composites. The trend of flexural modulus was the same as for the flexural strength, with the modulus value ranging from 1840.0 MPa to 2195.0 MPa. The addition of 0.7 wt% of PBI-HPG/RGO resulted in the maximum value in bending performance and tensile properties. The data showing the mechanical properties of neat and its composites is summarized in **Table 2**.

Table 2 The mechanical properties of epoxy composite.

PBI-HPG/RGO content	Impact strength (KJ/m ²)	Tensile strength (MPa)	Flexural strength (MPa)	Flexural modulus (MPa)
0.0 wt%	26.3±0.9	55.4±1.3	79.5±2.5	1840.0±40.0
0.1 wt%	30.3±1.3	63.8±0.6	102.9±0.4	2075.0±35.0
0.5 wt%	37.7±0.4	75.7±0.7	114.6±1.7	2140.0±28.0
0.7 wt%	39.6±0.5	90.0±0.3	121.6±1.3	2195.0±23.0
1.0 wt%	35.0±0.8	82.5±0.6	117.4±0.3	2180.0±31.0

Conclusions

This study synthesized a water-soluble perylene bisimide (PBI-HPG) and then a novel compound PBI-HPG/RGO was first synthesized via π - π stacking. The effects of PBI-HPG/RGO on the mechanical and thermal properties of epoxy composites were investigated. The results shown that PBI-HPG/RGO filler exhibit high enhancement effect for mechanical reinforcement of epoxy composites. The impact strength, tensile strength and flexural modulus of epoxy composite with 0.7 wt% PBI-HPG/RGO are 39.6 KJ/m², 90 MPa and 2195 Mpa (increased by 50.8%, 62.3% and 19.3%), respectively, compared with the neat epoxy resin. More important, the thermal degradation temperature, the glass transition temperature and thermal conductivity of epoxy composites also has been improved clearly.

Acknowledgements

The authors gratefully acknowledge the financial support by National Natural Science Foundation of China (51303034, 51163004 and 51463007), the Natural Science Foundation of Guangxi Province, China (2013GXNSFAA019308, 2014GXNSFDA118006 and 2014GXNSFBA118034), Guangxi Universities Scientific Research Project (No.YB2014165), Natural Science Foundation of Ningbo (No.Y40307DB05).

Notes and references

- C. S. Wu, Y. L. Liub and K. Y. Hsu, *Polymer*, 2003, **44**, 565-573.
- M. Flores, M. Morell, X. Fernández-Francos, F. Ferrando, X. Ramis and Á. Serra, *Eur. Polym. J.*, 2013, **49**, 1610-1620.
- N. Chikhi, S. Fellahi and M. Bakar, *Eur. Polym. J.*, 2002, **38**, 251-264.
- J. Liu, L. Tao, W. Yang, D. Li, C. Boyer, R. Wuhner, F. Braet and T. P. Davis, *Langmuir*, 2010, **26**, 10068-10075.
- L. Peng, Z. Xu, Z. Liu, Y. Wei, H. Sun, Z. Li, X. Zhao and C. Gao, *Nat. Commun.*, 2015, **6**, 5716.
- Y. Xu, K. Sheng, C. Li and G. Shi, *ACS Nano*, 2010, **4**, 4324-4330.
- Q. Liang, X. Yao, W. Wang, Y. Liu and C. P. Wong, *ACS Nano*, 2011, **5**, 2392-2401.

- Y. J. Wan, L. X. Gong, L. C. Tang, L. B. Wu and J. X. Jiang, *Composites Part A*, 2014, **64**, 79-89.
- B. Shen, W. Zhai, M. Tao, D. Lu and W. Zheng, *Compos. Sci. Technol.*, 2013, **77**, 87-94.
- S. Wang, B. M. Goh, K. K. Manga, Q. Bao, P. Yang and K. P. Loh, *ACS Nano. Organic*, 2010, **4**, 6180-6186.
- Y. Wang, J. Chen, Y. Chen, W. Li and C. Yu, *Anal. Chem.*, 2014, **86**, 4371-4378.
- L. Q. Xu, L. Wang, B. Zhang, C. H. Lim, Y. Chen, K. G. Neoh, E. T. Kang and G. D. Fu, *Polymer*, 2011, **52**, 2376-2383.
- S. Chen, Y. Liu, W. Qiu, X. Sun, Y. Ma and D. Zhu, *Chem. Mater.*, 2005, **17**, 2208-2215.
- L. Pan, S. Lu, X. Xiao, Z. He, C. Zeng, J. Gao and J. Yu, *RSC Adv.*, 2015, **5**, 3177-3186.
- D. Gorl, X. Zhang and F. Würthner, *Angew. Chem. Int. Ed. Engl.*, 2012, **51**, 6328-6348.
- D. Foix, Y. Yu, A. Serra, X. Ramis and J. M. Salla, *Eur. Polym. J.*, 2009, **45**, 1454-1466.
- H. Frey and R. Haag, *Mol. Biotech.*, 2002, **90**, 257-267.
- R. Haag and A. Sunder, *J. Am. Chem. Soc.*, 2000, **122**, 2954-2955.
- L. Ye, K. Letchford, M. Heller, R. Liggins, J. N. Kizhakkedathu, D. E. Brooks, Helen M. Burt, J. K. Jackson and D. Guan, *Biomacromolecules*, 2011, **12**, 145-155.
- R. K. Kainthan, C. Mugabe, H. M. Burt and D. E. Brooks, *Biomacromolecules*, 2008, **9**, 886-895.
- M. Adeli, N. Mirab, M. S. Alavidjeh, Z. Sobhani and F. Atyabi, *Polymer*, 2009, **50**, 3528-3536.
- Y. Xu, S. Leng, C. Xue, R. Sun, J. Pan, J. Ford and S. Jin, *Angew. Chem. Int. Ed. Engl.*, 2007, **46**, 3896-3899.
- Y. Wang, J. Chen, H. Jiao, Y. Chen, W. Li, Q. Zhang and C. Yu, *Chemistry*, 2013, **19**, 12846-12852.
- L. Zhou, B. He, J. Huang, Z. Cheng, X. Xu and C. Wei, *ACS Appl. Mater. Interfaces*, 2014, **6**, 7719-7727.
- C. Zen, S. Lu, L. Song, X. Xiao, J. Gao, L. Pan, Z. He and J. Yu, *RSC Adv.*, 2015, **5**, 35773-35782.
- M. Jonsson, D. Nyström, O. Nordin and E. Malmström, *Eur. Polym. J.*, 2009, **45**, 2374-2382.
- S. Movahedi, M. Adeli, A. K. Fard, M. Maleki, M. Sadeghizadeh and F. Bani, *Polymer*, 2013, **54**, 2917-2925.
- S. N. Tripathi, P. Saini, D. Gupta and V. Choudhary, *J. Mater. Sci.*, 2013, **48**, 6223-6232.
- T. A. Pham, N. A. Kumar and Y. T. Jeong, *Synth. Met.*, 2010, **160**, 2028-2036.
- C. Xu, R. S. Yuan and X. Wang, *New Carbon Mater.*, 2014, **29**, 61-66.
- C. Nethravathi and M. Rajamathi, *Carbon*, 2008, **46**, 1994-1998.
- Q. Guo, Z. Zheng, H. Gao, J. Ma and X. Qin, *J. Power Sources*, 2013, **240**, 149-154.
- G. Wang, Q. Tang, H. Bao, X. Li and G. Wang, *J. Power Sources*, 2013, **241**, 231-238.
- B. Wang and C. Yu, *Angew. Chem. Int. Ed. Engl.*, 2010, **49**, 1485-1488.
- A. M. Jastrzębska, E. Karwowska, A. R. Olszyna and A. Kunicki, *Surf. Coat. Technol.*, 2015, **271**, 225-233.
- D. Lee, S. H. Song, J. Hwang, S. H. Jin, K. H. Park, B. H. Kim, S. H. Hong and S. Jeon, *Small*, 2013, **9**, 2602-2610.
- S. H. Song, K. H. Park, B. H. Kim, Y. W. Choi, G. H. Jun, D. J. Lee, B. S. Kong, K. W. Paik and S. Jeon, *Adv. Mater.*, 2013, **25**, 732-737.
- L. Wang, L. Jiang, D. Su, C. Sun, M. Chen, K. Goh and Y. Chen, *J. Colloid. Interface Sci.*, 2014, **430**, 121-128.
- X. Zhang, K. Li, H. Li, J. Lu, Q. Fu and Y. Chu, *Synth. Met.*, 2014, **193**, 132-138.
- T. Kuilla, S. Bhadra, D. Yao, N. H. Kim, S. Bose and J. H. Lee, *Prog. Polym. Sci.*, 2010, **35**, 1350-1375.
- J. C. Meyer, A. K. Geim, M. I. Katsnelson, K. S. Novoselov, T. J. Booth and S. Roth, *Nature*, 2007, **446**, 60-63.
- T. Baumgärtel, S. Rehm, F. Würthner, C. von Borczyskowski and H. Graaf, *Appl. Surf. Sci.*, 2014, **318**, 51-58.
- L. Li, X. Zhang, J. Qiu, B. L. Weeks and S. Wang, *Nano. Energy*, 2013, **2**, 628-635.

ARTICLE

RSC Adv.

- 44 L. M. Veca, M. J. Meziani, W. Wang, X. Wang, F. Lu, P. Zhang, Y. Lin, R. Fee, J. W. Connell and Y. P. Sun, *Adv. Mater.*, 2009, **21**, 2088-2092.
- 45 Y. J. Wan, L. C. Tang, L. X. Gong, D. Yan, Y. B. Li and L. B. Wu, *Carbon*, 2014, **69**, 467-480.
- 46 Y. L. Liu, C. Y. Hsu, W. L. Wei and R. J. Jeng, *Polymer*, 2003, **44**, 5159-5167.
- 47 Y. Ni, S. Zheng and K. Nie, *Polymer*, 2004, **45**, 5557-5568.
- 48 R. Liu and X. Wang, *Polymer Degrad. Stab.*, 2009, **94**, 617-624.
- 49 L.C. Tang, Y.J. Wan, D. Yan, Y. B. Pei, L. Zhao and Y. B. Li, *Carbon*, 2013, **60**, 16-27.
- 50 S. Y. Yang, W. N. Lin, Y. L. Huang, H. W. Tien, J. Y. Wang, C. C. M. Ma, S. M. Li and Y. S. Wang, *Carbon*, 2011, **49**, 793-803.
- 51 X. Wang, L. X. Gong, L. C. Tang, K. Peng, Y. B. Pei and L. Zhao, *Compos. Part A*, 2015, **69**, 288-298.
- 52 R. Thomas, D. Yumei, H. Yuelong, Y. Le, P. Moldenaers, Y. Weimin, T. Czigany and S. Thomas, *Polymer*, 2008, **49**, 278-294.
- 53 M. T. Bashar, U. Sundararaj and P. Mertiny, *Polym Eng. Sci.*, 2014, **54**, 1047-1055.